Bioactive Materials 19 (2023) 474–485

Contents lists available at ScienceDirect

Bioactive Materials

journal homepage: www.keaipublishing.com/en/journals/bioactive-materials

Regulated macrophage immune microenvironment in 3D printed scaffolds for bone tumor postoperative treatment

Cuidi Li [a,1], Changwei Li [a,1], Zhenjiang Ma [b,1], Hongfang Chen [b], Huitong Ruan [a], Lianfu Deng [a], Jinwu Wang [b,**], Wenguo Cui [a,*]

[a] Department of Orthopaedics, Shanghai Key Laboratory for Prevention and Treatment of Bone and Joint Diseases, Shanghai Institute of Traumatology and Orthopaedics, Ruijin Hospital, Shanghai Jiao Tong University School of Medicine, Shanghai, 200025, PR China

[b] Shanghai Key Laboratory of Orthopedic Implant, Department of Orthopedic Surgery, Shanghai Ninth People's Hospital Affiliated Shanghai Jiao Tong University School of Medicine, Shanghai, 200011, PR China

ARTICLE INFO

Keywords:
3D printing
Drug delivery
Microenvironment
Macrophage polarization
Bone regeneration

ABSTRACT

The 3D printing technique is suitable for patient-specific implant preparation for bone repair after bone tumor resection. However, improving the survival rate due to tumor recurrence remains a challenge for implants. The macrophage polarization induction to M2-type tumor-associated macrophages (TAMs) by the tumor microenvironment is a key factor of immunosuppression and tumor recurrence. In this study, a regenerative scaffold regulating the macrophage immune microenvironment and promoting bone regeneration in a dual-stage process for the postoperative treatment of bone tumors was constructed by binding a colony-stimulating factor 1 receptor (CSF-1R) inhibitor GW2580 onto in situ cosslinked hydroxybutylchitosan (HBC)/oxidized chondroitin sulfate (OCS) hydrogel layer covering a 3D printed calcium phosphate scaffold based on electrostatic interaction. The hydrogel layer on scaffold surface not only supplied abundant sulfonic acid groups for stable loading of the inhibitor, but also acted as the cover mask protecting the bone repair part from exposure to unhealthy growth factors in the microenvironment at the early treatment stage. With local prolonged release of inhibitor being realized via the functional material design, CSF-1R, the main pathway that induces polarization of TAMs, can be efficiently blocked, thus regulating the immunosuppressive microenvironment and inhibiting tumor development at a low therapeutic dose. At the later stage of treatment, calcium phosphate component of the scaffold can facilitate the repair of bone defects caused by tumor excision. In conclusion, the difunctional 3D printed bone repair scaffold regulating immune microenvironment in stages proposed a novel approach for bone tumor postoperative treatment.

1. Introduction

With the development of 3D printing technology, bone defects caused by tumors can be gradually repaired using printed implants with customized shapes [1–4]. However, malignant tumors such as osteosarcoma, are prone to recurrence and cause a low survival rate [5,6], which is difficult to be improved by a single bone repair implant. The role of macrophage in tumor development and recurrence has recently been topical in research [7,8]. Macrophages exist in different tumor types and can phagocytose cancer cells [6,9]. However, in the tumor microenvironment containing high levels of macrophage colony-stimulating factor (MCSF), macrophages can be recruited and induced to M2-polarized tumor-associated macrophages (TAMs), causing immunosuppression and promoting tumor development [10–12]. Therefore, design of 3D printed scaffolds functionally regulate macrophage behavior in the tumor microenvironment may provide a new approach for the bone tumor postoperative therapy [13–15].

Macrophages have phenotypes that change in response to external stimuli [16–18]. The classic M1-type macrophages initiate pro-inflammatory cytokine responses, which can not only directly

Peer review under responsibility of KeAi Communications Co., Ltd.
* Corresponding author.
** Corresponding author.
E-mail addresses: wangjw@sjtu.edu.cn (J. Wang), wgcui80@hotmail.com (W. Cui).
[1] These authors contributed equally to this work.

https://doi.org/10.1016/j.bioactmat.2022.04.028
Received 6 February 2022; Received in revised form 31 March 2022; Accepted 25 April 2022

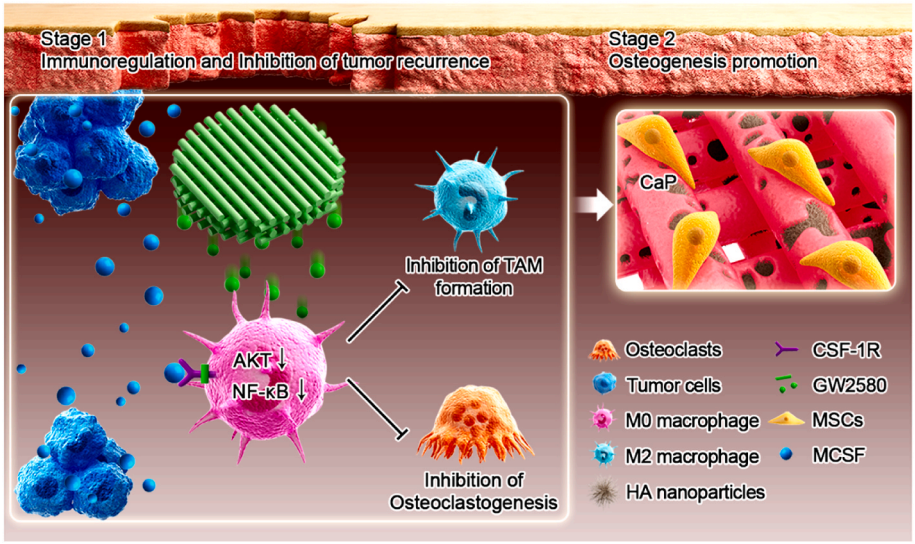

Scheme 1. Schematic demonstrates function process and mechanism of the 3D printed scaffold regulating macrophage immune microenvironment for postoperative treatment of bone tumors.

phagocytose cancer cells, but also promote tumor killer T-helper 1 cell response by participating in high-efficiency antigen delivery to inhibit tumor development [19,20]. In contrast, M2-type macrophages are often associated with poor prognosis [9,21]. After the CSF-1R on macrophage surface binds to the MCSF secreted by tumor cells, macrophages are polarized to TAMs, which promote tumor cells' development and metastasis [10,19,22]. Therefore, the CSF-1R pathway is a key target of macrophage behavior regulation in the tumor microenvironment [19]. As reported previously, CSF-1R inhibitors can reprogram macrophage function, reduce the local TAMs cells number, and promote M1-type repolarization, thereby alleviating the unhealthy tumor microenvironment [19]. However, the release behavior of the CSF-1R inhibitor has been demonstrated to significantly affect its immunoregulation and tumor inhibition effect [23]. During treatment, inhibitors need to be released in a sustained manner. Thus, the design and preparation of 3D printed scaffolds functionally releasing CSF-1R inhibitors are expected to inhibit tumor recurrence and promote bone defect repair by regulating local macrophage behavior [24–26].

Inspired by the interaction between macrophages and cancer cells, a customized difunctional regenerative scaffold regulating the local macrophage behavior in the tumor microenvironment was constructed by loading the CSF-1R inhibitor GW3580 onto in situ cosslinked hydroxybutylchitosan (HBC)/oxidized chondroitin sulfate (OCS) hydrogel layer covering a 3D printed self-setting calcium phosphate scaffold based on electrostatic interaction (Scheme 1). Self-setting calcium phosphate ceramic (CPC) has been applied in clinical bone repair and exhibited good integration [27]. In this study, the CPC-based bio-ink displayed good formability for bone repair scaffold printing. The hydrogel layer on scaffold surface can not only supply abundant sulfonic acid groups for stable loading of the inhibitor, but also act as the cover mask protecting the bone repair part from exposure to unhealthy growth factors in the microenvironment at the early stage of treatment. *In vitro* study indicated that gradually released GW2580 from the scaffold efficiently blocked the CSF-1R and NF-κB pathways, thus, significantly inhibited both the M2-type polarization of macrophages and osteoclast differentiation from monocytes. At late stage of GW2580 release, the CPC-based scaffolds showed regular properties to promote the osteogenic differentiation of bone marrow mesenchymal stem cells (BMSCs). Furthermore, *in vivo* experiments demonstrated that the regenerative scaffold gradually releasing GW2580 effectively reduced the proportion of M2-type macrophages in the tumor and inhibited tumor growth after implantation near the tumor at a low therapeutic dose, without affecting general behavior and survival of the animals.

2. Materials and methods

2.1. Synthesis of materials for 3D printing

HBC [28,29], OCS [30], and methylacrylate hyaluronic acid (HAMA) [31] were prepared as described previously. The products were separately dialyzed with distilled water, lyophilized and stored at 4 °C.

2.2. 3D printing of CPC scaffolds

CPC scaffolds were printed as previously reported [32]. CPC powders (Rebone, Shanghai, China) were evenly mixed with 5 wt% HAMA aqueous solution (containing 0.5% w/v lithium based photoinitiator) at an optimized solid-liquid ratio to prepare the printable bio-ink. Scaffolds were printed using a 3D bioprinter (Cellink, Gothernburg, Sweden) at room temperature, post-crosslinked via visible light (405 nm) irradiation for 30 s, and immersed overnight in deionized water at 37 °C for hydration. Next, the scaffolds were dried and collected for further use. Scaffolds for *in vitro* experiments were printed into a cuboid shape (side length = 10 mm; height = 2 mm). Scaffolds for the *in vivo* experiment were printed into a disc shape (diameter = 8 mm; height = 2 mm).

2.3. Fabrication and characterization of inhibitor loaded scaffold

HBC solutions (1 wt%, 2 wt%, 4 wt%) were prepared, dropped on the scaffolds, and allowed to infiltrate for 15 min. Subsequently, the macropores interconnection in the scaffolds were assessed to optimize the concentration of the HBC solution for scaffold coating. Next, the OCS solution (40 mg/mL) was dropped onto the scaffolds for in situ crosslinking with the HBC solution. The CPC scaffolds coated with the HBC/OCS hydrogel (CPC/hydrogel) were dried at room temperature. The CPC and CPC/hydrogel scaffolds morphologies were assayed using a scanning electron microscope (SEM; TESCAN Inc Warrendale, PA, USA) to verify the coating effect of the in situ crosslinked hydrogel. Furthermore, CPC/hydrogel scaffolds were assayed using a microscopic imaging infrared spectrometer (Thermofisher, Waltham, MA, USA) and an energy dispersive spectroscopy (EDS; TESCAN Inc).

To prepare the inhibitor loaded scaffolds, GW2580 (MedChemExpress, NJ, USA) was dissolved in dimethylsulfoxide at 10 mM as stock solution, diluted to a certain concentration according to experiment

contents and dropped onto the hydrogel coated scaffolds (100 μL per scaffold). After incubating at room temperature for 120 min, the scaffolds were dried and stored at 4 °C until use. For most *in vitro* experiments, 10 μM GW2580 solution was dropped onto each printed scaffold to prepare the inhibitor loaded scaffold. In the macrophage polarization experiment, printed scaffolds loaded with 10 μM and 100 μM GW2580 solution were prepared separately as the low and high dose group.

2.4. GW2580 release from scaffolds

CPC/hydrogel/GW2580 scaffolds were prepared as mentioned above. CPC scaffolds loaded with same dosage of GW2580 were prepared as control group. The scaffolds were then placed in 2 mL phosphate buffer saline (PBS) each in 12 well culture plate and incubated at 37 °C. After a standard curve of GW2580 solution being established (Fig. S1), the supernatant in each well was extracted for absorbance detection at 283 nm by an ultraviolet spectrophotometer (Eppendorf, Germany) at set time points. Equal amount of fresh PBS was added each time to continue the experiment. Afterwards, GW2580 concentration was calculated for release ratio analysis.

2.5. Extract preparation

The extracts of CPC, CPC/hydrogel, and CPC/hydrogel/GW2580 scaffold were prepared as previous report [33]. First, each of the scaffolds was put into a well in 24 well plate. Next, 1 mL of conditioned culture medium was added and thermostatically incubated for 24 h. Afterwards, the supernatant was extracted and stored at 4 °C until use. The conditioned medium used to assay the effect of extracts on the inhibition of pathways was standard culture medium (alpha minimal essential medium [α-MEM] containing 10% fetal bovine serum [FBS] and 1% penicillin/streptomycin). A standard culture medium containing 30 ng/mL MCSF (PeproTech, USA) was used as the conditioned medium to assay the effect of extracts on mouse bone marrow-derived monocyte (BMM) proliferation. An osteoclast-differentiation inducing medium containing 30 ng/mL MCSF and 100 ng/mL receptor activator for nuclear factor-κB ligand (RANKL; PeproTech) was prepared before the experiment and used as the conditioned medium to assess the effect of extracts on osteoclast differentiation. A polarization-inducing medium containing 20 ng/mL IL-10, IL-4, and MCSF (Peprotech) was used as the conditioned medium to evaluate the effects of the extract on the M2 polarization of BMMs. The osteogenic differentiation-inducing medium (Cyagen Biosciences, Jiangsu, China) was used as the conditioning medium to assess effects of the extract on osteogenic differentiation of mesenchymal stem cells.

2.6. Ions concentration in the scaffold extract medium

The extract medium of CPC, CPC/hydrogel and CPC/hydrogel/GW2580 scaffolds was prepared as described above with α-MEM. After incubating for 24 h, the scaffold extract medium was collected respectively. Fresh α-MEM was used as blank control. The concentration of phosphorous and sulfide ions in the medium was detected with an inductive coupled plasma emission spectrometer (Thermo Fisher Scientific, USA).

2.7. Western blot assay for inhibition of pathways study

First, RAW264.7 cells were seeded in six-well plates at 8×10^5 cells/well and incubated with the scaffolds extracted culture medium for 4 h. Next, the cells were cultured with a standard culture medium for 24 h, stimulated with medium containing 10 ng/mL MCSF for 2 h, and processed for protein extraction and subsequent concentration measurement. Western blot assay was then performed to detect content of Phospho CSF1R, CSF1R, phospho-AKT, total AKT, phospho–NF–κB, total NF-κB, phospho-ERK, total ERK, and actin antibodies (Sangon Biotech, Shanghai, China) in the samples. The results were quantified using Image J software (National Institute of Health, USA).

2.8. Inhibition of proliferation and osteoclastogenesis of BMMs

BMMs were extracted and cultured as previous report [34,35]. First, the effects of the extract medium on BMMs proliferation were investigated. 1×10^4 BMMs were evenly seeded into each well of a 96-well plate and incubated with the scaffold extract medium separately. Cell viability was analyzed after 24 and 72 h of culture using the Cell Counting kit-8 (CCK-8) assay kit. Cells cultured in standard media containing 30 ng/mL MCSF were used as control group.

The effects of scaffold extract medium on osteoclastogenic cells were subsequently assayed. Osteoclast differentiation-inducing medium was prepared before the experiment. Scaffold extract medium were prepared by incubating the scaffolds with an osteoclast differentiation-inducing medium as described above. 1×10^4 BMMs were evenly seeded into each well of a 96-well plate and incubated with the scaffold extract medium separately. A standard osteoclast-inducing differentiation medium was used as the control. The medium was refreshed every 72 h. After 24 and 72 h of culture, cells were fixed using 4% paraformaldehyde (PFA) and stained using a tartrate-resistant phosphatase (TRAP) kit (Sigma-Aldrich), and TRAP-positive osteoclasts were observed using an optical microscope (Leica, Weztlar, Germany). The TRAP-positive cell area was calculated with the Image J software. Furthermore, cells were stained with 2-(4-Amidinophenyl)-6-indolecarbamidine dihydrochloride (DAPI) and rhodamine-phalloidin (Sigma-Aldrich) and the cell morphology was observed under a confocal laser scanning microscope (Carl Zeiss AG, Bena, Germany).

2.9. Inhibition of M2 polarization of BMMs

The M2 phenotype polarization inducing medium containing 20 ng/mL MCSF, IL-4, and IL-10 was prepared 1 h before the experiment. Scaffold extract medium was prepared by incubating the scaffolds with a polarization-inducing medium as described above. 5×10^4 BMMs were evenly seeded into each well of a 24 well plate and incubated with scaffold extract medium separately. After 24 h of culture, cells were collected for analysis. The specific marker expression of M1 macrophages (IL-1β, inducible nitric oxide synthase (iNOs)), and M2 macrophages (CD163 and CD206) was analyzed via real-time reverse transcriptive polymerase chain reaction (RT-PCR). The M2 macrophage phenotype proportion was further assessed by a flow cytometer after staining the specific marker CD206.

2.10. Effects on BMSCs function

The effect of scaffolds at the later stage of GW2580 release on proliferation, adhesion, and osteogenic differentiation of mouse BMSCs (mBMSCs) was analyzed. The CPC, CPC/hydrogel, and CPC/hydrogel/GW2580 scaffolds were put separately into a 24 well culture plate (each in a well) and incubated with 1 mL of standard culture medium. The medium was refreshed daily. After 7 days of incubation, scaffolds were collected for following study. mBMSCs were isolated as previous report [36]. 1×10^4 mBMSCs were seeded onto each scaffold in a 24-well plate and cultured for 24 and 72 h. Cell viability was then assayed with a CCK-8 kit to test the effect of scaffolds on cell proliferation. Cells cultured in standard medium were used as controls.

To assay cell adhesion on the scaffolds, mBMSCs were evenly seeded onto each scaffold (1×10^4 per scaffold) and co-cultured for 3 days; cell morphology on the scaffolds was detected with a confocal laser scanning microscopy (Zeiss) after fixing, staining with rhodamine-phalloidin and DAPI. To assess the effect of scaffolds on cell function, mBMSCs were evenly seeded into a 24-well plates (5×10^4 per well), cultured with the scaffold extract medium separately for seven days. Then, the cells were fixed, stained with an alkaline phosphatase (ALP) kit (Beyotime,

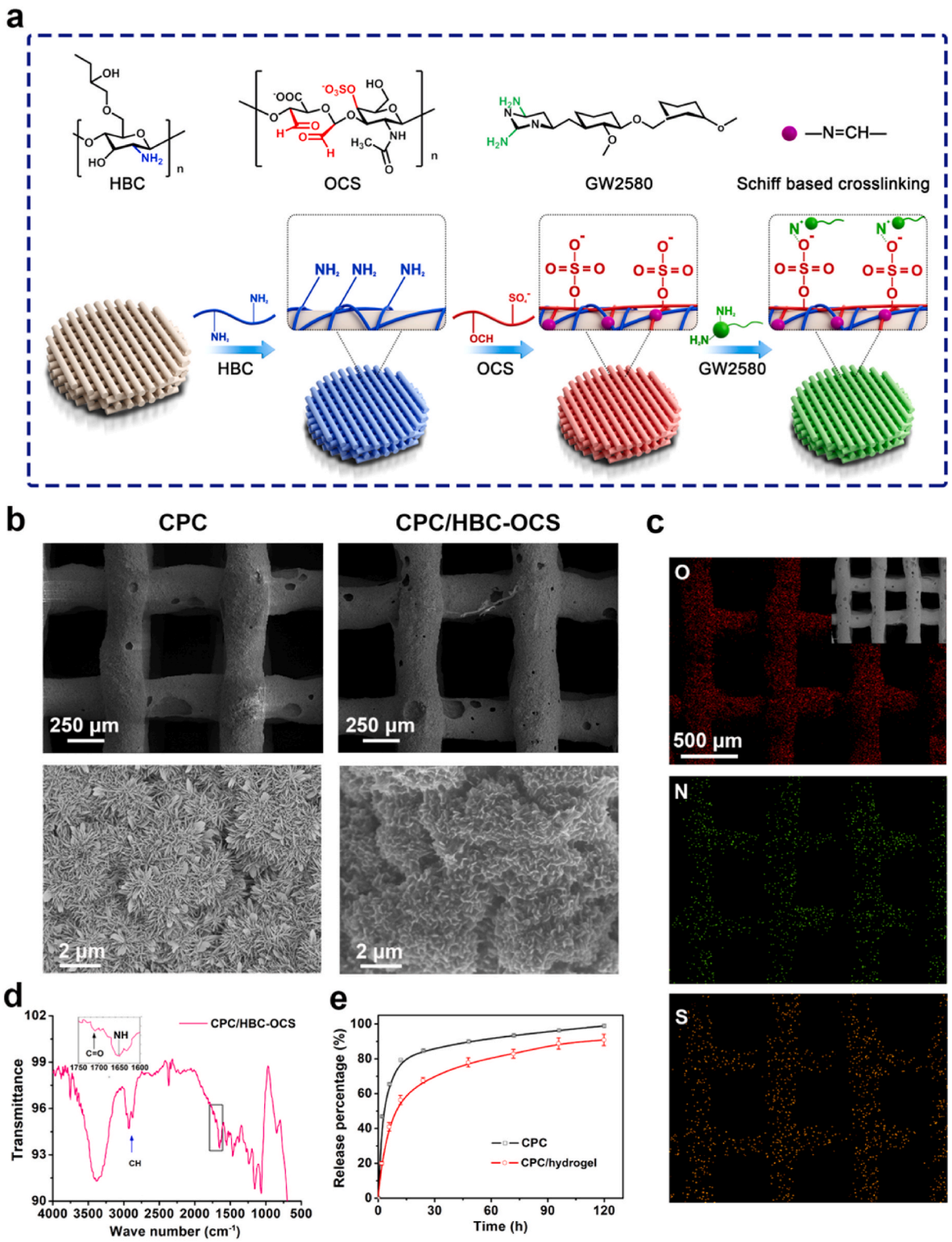

Fig. 1. Design of an inhibitor-loaded scaffold. (a) Schematic shows preparation process and related mechanism of the inhibitor-loaded scaffold. (b) SEM images show pore structure and surface morphology of CPC and CPC/HBC-OCS scaffolds. (c) EDS images show coating efficiency of HBC-OCS hydrogel on CPC scaffolds. (d) Microscopic infrared spectra of the CPC/HBC-OCS scaffold. (e) GW2580 release ratio from CPC and CPC/HBC-OCS scaffolds in 120 h (n = 3).

Shanghai, China), and observed under an optical microscope (Leica).

2.11. Anti-tumor efficacy in murine 4T1 breast cancer model

Eighteen healthy female BALB/c mice (four-week old, 20 g) were obtained from Shanghai Jihui Laboratory Animal Co., Ltd. (Shanghai, China) and divided into three experimental groups: (1) untreated, (2) CPC, and (3) CPC/hydrogel/GW2580 (GW2580: 50 mg/kg). Luc-4T1 breast cancer cells (1×10^5) were injected subcutaneously into the groin of each mouse. Implantation therapy was initiated when the average tumor volume approached 100 mm^3. The mice were anaesthetized with pentobarbital (1 mL/kg), and the scaffolds were implanted

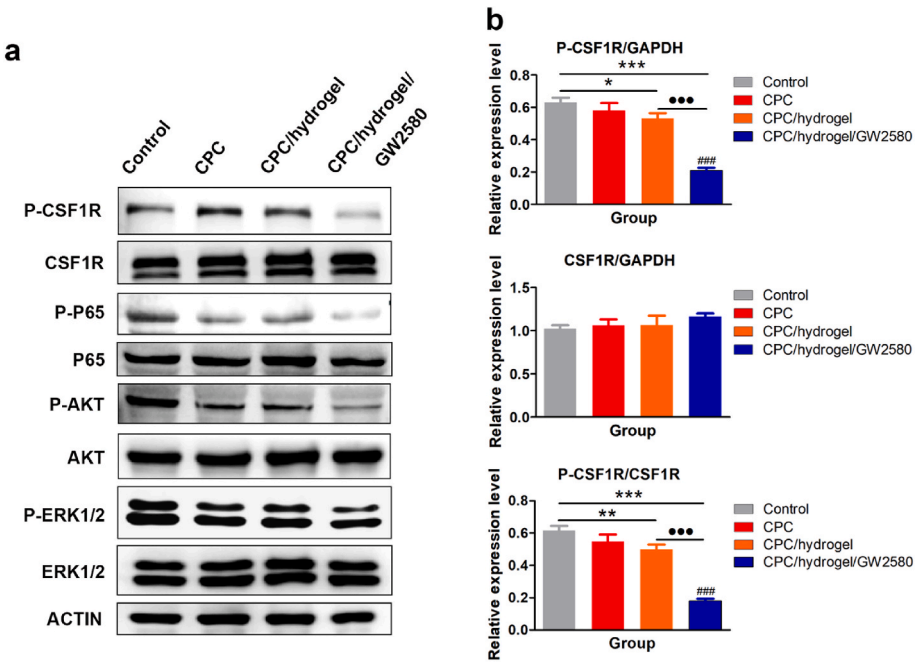

Fig. 2. Released components inhibit CSF-1R and downstream pathways. (a) Cropped blots and (b) related quantification results of Western blot assay show the effect of released components from scaffolds on signaling pathways inhibition (n = 3, $^{*}P < 0.05$, $^{**}P < 0.01$, $^{***}P < 0.001$ vs. control; $\#\#\#P < 0.001$ vs. CPC group; $\bullet\bullet\bullet P < 0.001$ vs. CPC/hydrogel group by one-way ANOVA).

subcutaneously near the tumor. Tumor volume was measured by palpation and *in vivo* imaging system (IVIS, PerkinElmer, Waltham, MA, US) after injection of 100 μL d-luciferin substrate solution respectively. Mice body weight was measured every alternate day. The animals were sacrificed after 10 days of implantation; the tumors and scaffolds were collected and processed for analysis. The animal experiments were performed following the guidelines and regulations of the Institutional Animal Care and Use Committee of Ruijin Hospital, Shanghai Jiao Tong University School of Medicine.

2.12. FACS analysis of tumor samples

The harvested tumor tissues were processed for single-cell suspension preparation according to a reported procedure [19]. The expression of CD86 and CD206 was evaluated to identify the percentage of M1 and M2 macrophages in the tumor after $CD11b^{+}$ macrophage isolation and phenotype quantification.

2.13. Histological analysis

Tumor samples were fixed in 4% PFA and processed into sections to analyze the local macrophage phenotype. Immunofluorescence staining against iNOs and CD206 was performed and subsequently observed under a confocal microscope (Zeiss). To quantitatively evaluate the polarized macrophages, the Image J software was used to calculate the mean fluorescence intensity.

2.14. Statistical analyses

Data are presented as the means ± standard deviations. GraphPad Prism software was used to do the statistical analyses among different groups.

3. Result and discussion

3.1. Characteristic of inhibitor loaded scaffolds

As previously described, the CPC-based bioink was prepared and fed into a 3D printer to prepare the bone repair scaffolds [33]. A photo-crosslinkable HAMA solution was introduced into the bio-ink for formability promotion after scaffold printing. In an aqueous environment, the inorganic component calcium phosphate cement would gradually set into biodegradable hydroxyapatite, which is similar to the main component of bone and promotes osseointegration [37,38]. The HBC solution was first assembled onto the scaffolds to bring amine groups. The OCS solution was then crosslinked in situ with HBC to provide sulfonic acid groups for the subsequent loading of inhibitor GW2580 on the scaffolds (Fig. 1a).

SEM and EDS assays were performed to analyze the HBC/OCS hydrogel coating efficiency on the scaffolds. Fig. 1b shows that the pore sizes of CPC and CPC/hydrogel scaffolds are approximately 500 μm and are ideal for bone tissue regeneration. Printed CPC scaffolds were subjected to a hydration process for complete setting and mechanical strength improvement. Correspondingly, the hydrated CPC scaffolds were covered with needle-like hydroxyapatite nanoparticles on the surface (Fig. 1b). At optimum concentration and assembly process of HBC and OCS, pore connectivity and structure of the scaffolds were not affected by the hydrogel coating. The HBC/OCS hydrogel evenly covered the hydroxyapatite layer as a thin mask shield on the surface of the CPC/hydrogel scaffolds. According to the EDS mapping results (Fig. 1c), Nitrogen (N) element in HBC, sulfur (S) element in OCS and the oxygen (O) existing in both HBC and OCS show a similar and even distribution of macroporous structure in scaffolds, verifying the HBC/OCS hydrogel fine coating. The groups of HBC and OCS on the scaffolds were analyzed using a microscopic imaging infrared spectrometer (Fig. 1d). According to the results, the peaks of the N–H and C═O groups were detected around 1650 cm^{-1} and 1715.3 cm^{-1}, respectively, indicating the successful assembling of HBC and OCS, and remaining free aldehyde groups on the OCS molecular chain.

To prolong the inhibitor release time, GW2580 was designed to bind

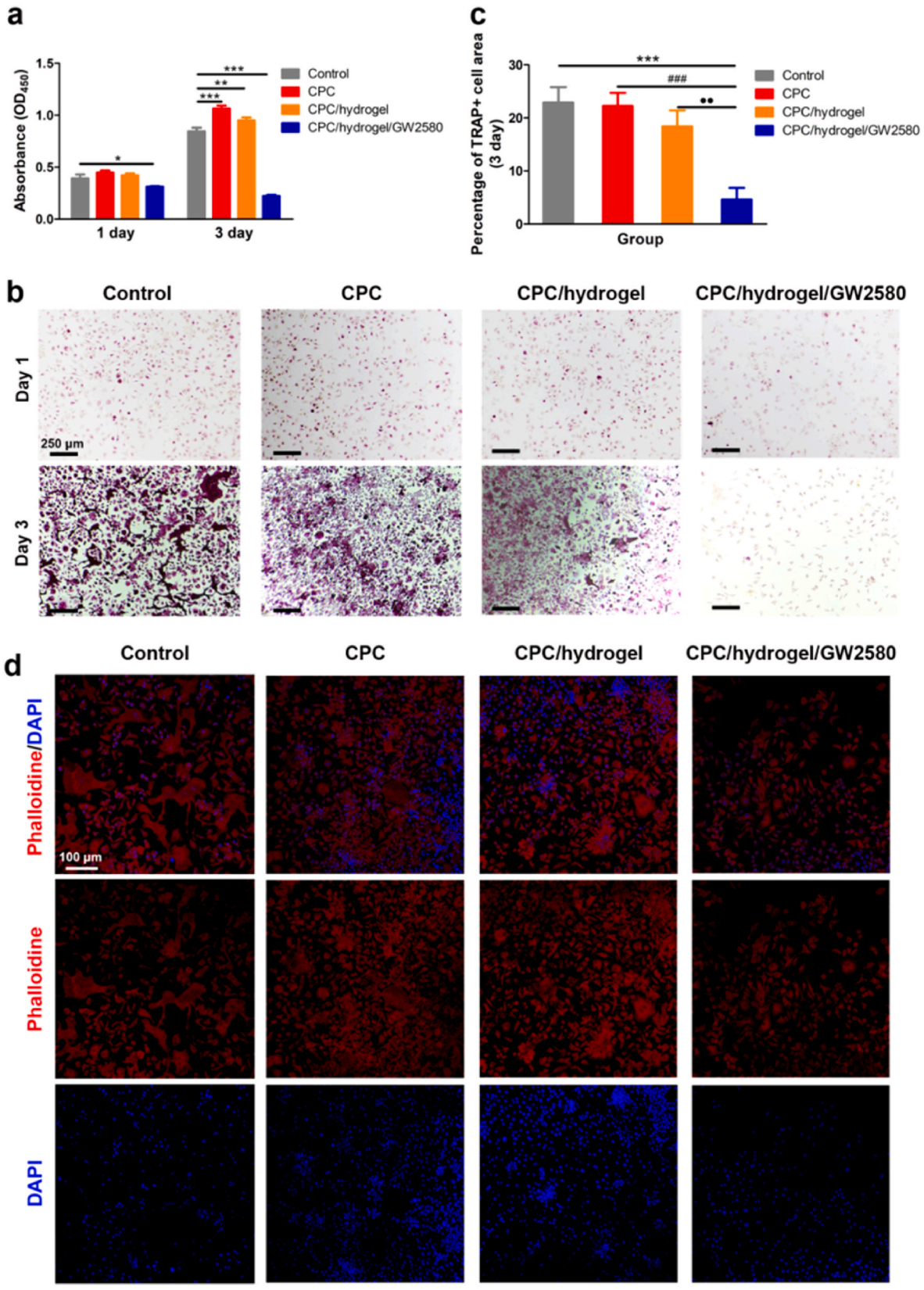

Fig. 3. Released components inhibit proliferation and osteoclastogenesis of BMMs. (a) Effect of released components from scaffolds on BMMs proliferation after 1 and 3 days of culture. (n = 3, $^{*}P < 0.05$, $^{**}P < 0.01$, $^{***}P < 0.001$ vs. control by one-way ANOVA). (b) TRAP staining images and (c) related quantification results show the effect of released components on BMMs osteoclastogenesis after 1 and 3 days of culture. (n = 3, $^{***}P < 0.001$ vs. control; $^{\#\#\#}P < 0.001$ vs. CPC group; ●●$P < 0.01$ vs. CPC/hydrogel group by one-way ANOVA). (d) Confocal microscope images show morphology of BMMs in scaffold extract medium after 3 days of culture.

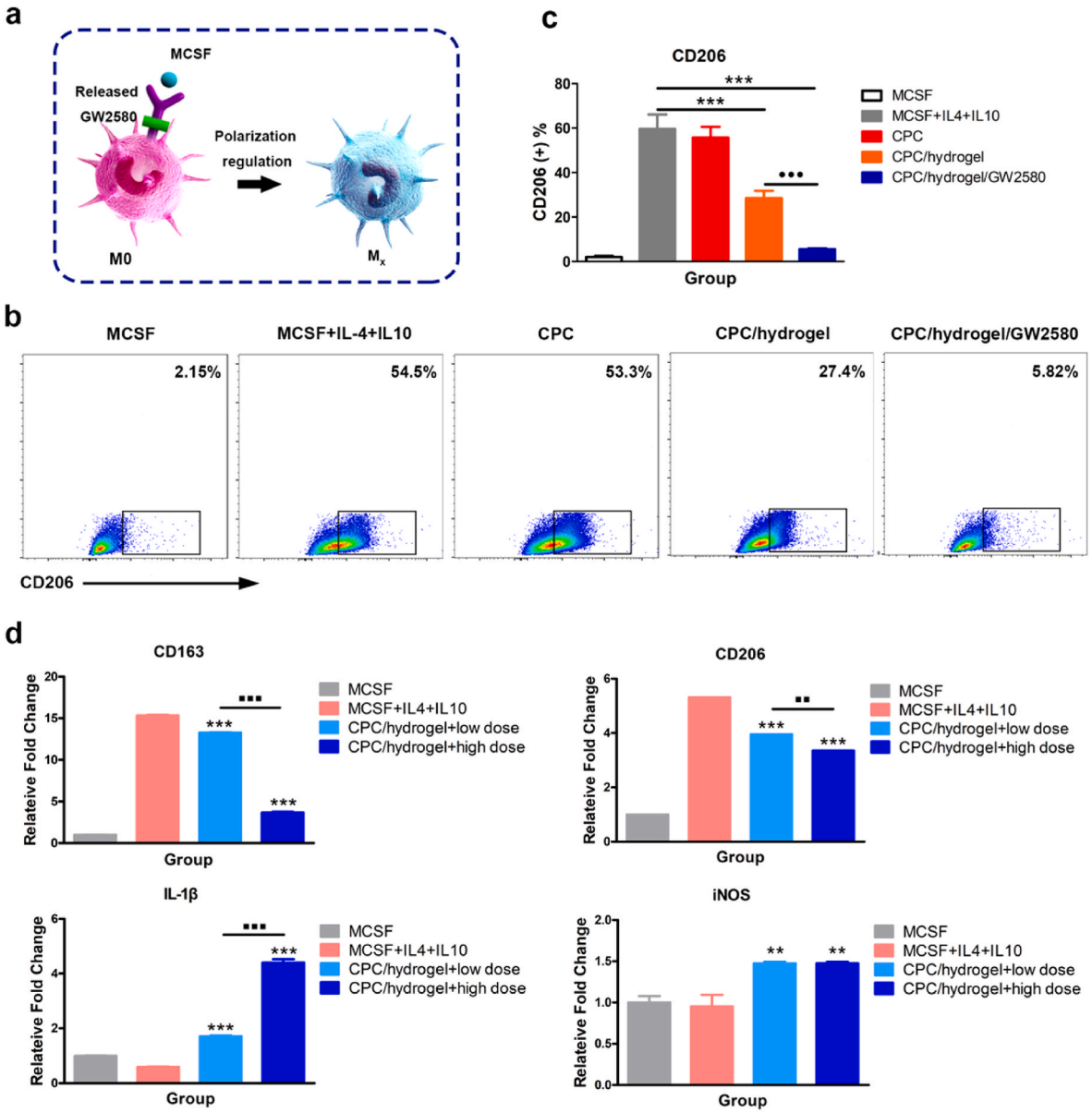

Fig. 4. Released components regulate polarization of macrophages. (a) Schematic shows the process of released components regulating polarization of macrophages. (b) FACS assay images and (c) statistical analysis results demonstrate the effect of scaffold extract medium on marker expression ($CD206^{+}$) of M2-type macrophages. (n = 3, ***$P < 0.001$ vs. MCSF + IL4+IL10 group; ●●●$P < 0.001$ vs. CPC/hydrogel group by one-way ANOVA). (d) RT-PCR results show the effect of released components from scaffolds on genes expression of M1 (IL-1β, iNOs) and M2 (CD163, CD206) type macrophages (n = 3, **$P < 0.01$, ***$P < 0.001$ vs. MCSF + IL4+IL10 group; ■■$P < 0.01$, ■■■$P < 0.001$ vs. CPC/hydrogel + low dose group by one-way ANOVA).

on scaffolds through electrostatic interaction. According to the microscopic infrared spectrum results, some of the inhibitor could also in situ crosslink with OCS via schiff-base reaction. Calculated release ratio curves (Fig. 1e) indicated the release rate of GW2580 was effectively slowed on CPC/hydrogel scaffolds, compared with on the CPC scaffolds. The inhibitor was found to gradually release from the hydrogel coated scaffolds in one week.

3.2. Inhibition of signaling pathways

MCSF is a key cytokine responsible for proliferation and differentiation of macrophages [39]. Abundant MCSF in the tumor microenvironment is associated with the recruitment and polarization of M2-like TAMs, which led to localized immunosuppression, growth and metastasis of cancer cells [40–42]. Therefore, high levels of MCSF are associated to a poor prognosis of bone tumors [43]. In this study, the CSF-1R inhibitor GW2580 was designed to be loaded on a CPC scaffold based on electrostatic interactions between amidogen (GW2580) and sulfonic acid (OCS) groups. After incubation in a microenvironment rich in growth factors, the competitive interaction between the factors and OCS could promote the release of GW2580, which inhibited the CSF-1R signaling pathway and sequentially regulated the immune microenvironment. Therefore, the effect of GW2580 release on the inhibition of CSF-1R signaling was first investigated.

After incubating with the extract medium of CPC, CPC/hydrogel, and CPC/hydrogel/GW2580 scaffolds separately for 4 h, macrophages were normally cultured for 24 h and stimulated with the medium containing MCSF for 2 h before the Western blot assay. According to results shown in Fig. 2, the extract medium containing released GW2580 exhibited an efficient inhibition of phosphorylation of CSF-1R at 24 h ($P < 0.001$). Furthermore, the phosphorylation of AKT and NF-κB signaling pathways were also significantly ablated by the released GW2580. As is known,

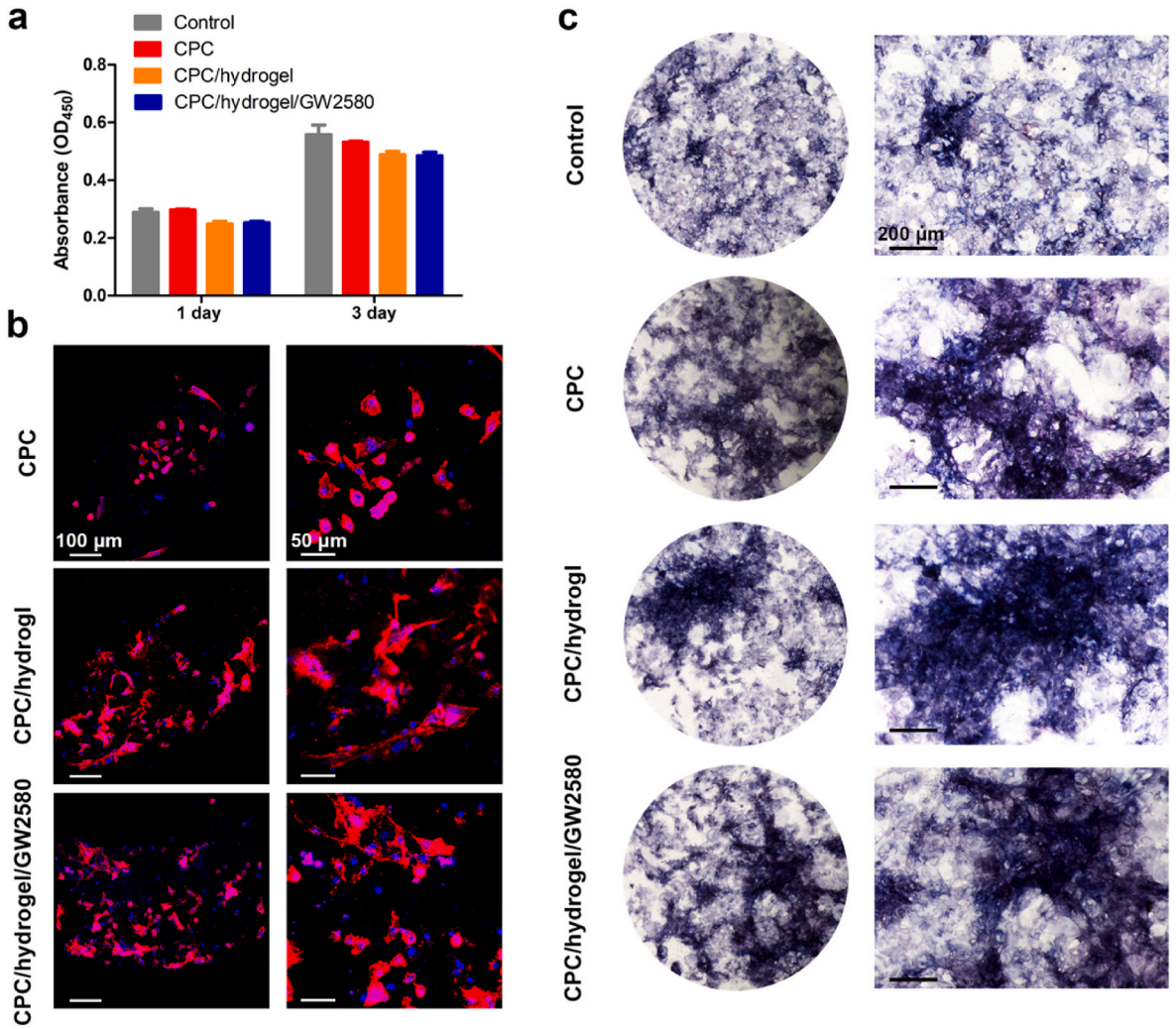

Fig. 5. Effect of GW2580-loaded scaffolds on mBMSCs function at late stage of inhibitor release. (a) CCK-8 assay results show the effect of scaffolds on mBMSCs proliferation after 1 and 3 days of culture (n = 3). (b) Confocal microscope images show mBMSCs morphology on CPC, CPC/hydrogel and CPC/hydrogel/GW2580 scaffolds after 3 days of coculture. (c) ALP staining images show the effect of scaffold extract medium on osteogenic differentiation of mBMSCs after 7 days of culture.

the activation of NF-κB and AKT pathways is essential in the progression of aggressive malignancies [44,45].

3.3. Inhibition of osteoclastogenesis

Osteoclastogenesis, the leading cause of bone destruction, is closely related to the activation of CSF-1R and NF-κB signaling pathways [43,46]. Especially, MCSF is known to promote both growth and osteoclast differentiation of mononuclear macrophages by binding to its receptor on cell-surface [47]. Once osteoclasts were activated in the tumor microenvironment and start to destroy the bone matrix, growth factors further enhancing tumor growth would be released [48,49]. Based on the results in section 3.2, it was speculated that the GW2580 loaded scaffolds may obtain the potential to inhibit osteoclastogenesis, and thus block the important link in the vicious cycle of tumor recurrence and metastasis [50].

Herein, the effects of scaffold extracts on BMMs proliferation and osteoclastogenesis were carefully analyzed. In previous studies, GW2580 was reported to inhibit the proliferation of MCSF-dependent cells such as monocytes [47]. Therefore, the concentration-dependent inhibition effect of dissociative GW2580 was verified first (data not shown). After that, GW2580 was loaded onto the scaffolds at an effective concentration. The viability of BMMs cultured in scaffold extracts was assayed using a CCK-8 kit after 12 and 72 h of co-culture. Fig. 3a shows the proliferation of BMMs cultured in the extract medium of CPC/hydrogel/GW2580 scaffolds is significantly inhibited ($P < 0.001$). The results confirmed that released GW2580 from the scaffolds worked the same as the dissociative ones.

The effect of scaffold extract medium on osteoclastogenesis of BMMs was then analyzed by TRAP staining after 1 and 3 days of co-culture. Consistent with our speculation, Fig. 3b and c shows that osteoclastogenesis of BMMs is completely inhibited in the CPC/hydrogel/GW2580 extract medium ($P < 0.001$). TRAP-positive osteoclasts were hardly detected after 3 days of co-culture. Additionally, cell morphology observation under a confocal microscope confirmed the TRAP staining results (Fig. 3d). Induced multi-nucleated osteoclasts were found in the control group after 3 days of culture but were not detected in the CPC/hydrogel/GW2580 group.

Unexpectedly, the extracts of CPC/hydrogel scaffolds partially blocked the CSF-1R signaling pathway and inhibited osteoclastogenesis ($P < 0.001$). Therefore, we collected the scaffolds release medium and analyzed the N and S ion concentrations. The results indicated that HBC and OCS were released from the scaffolds during the extraction process (Fig. S2). Although the mechanisms were not understood, it was hypothesized that the inhibitory effect might be related to the release of OCS, which interacted with growth factors such as MCSF and RANKL in the inducing medium, interfering with the interaction of the signaling molecules. In previous studies, CS was reported to suppress osteoclast

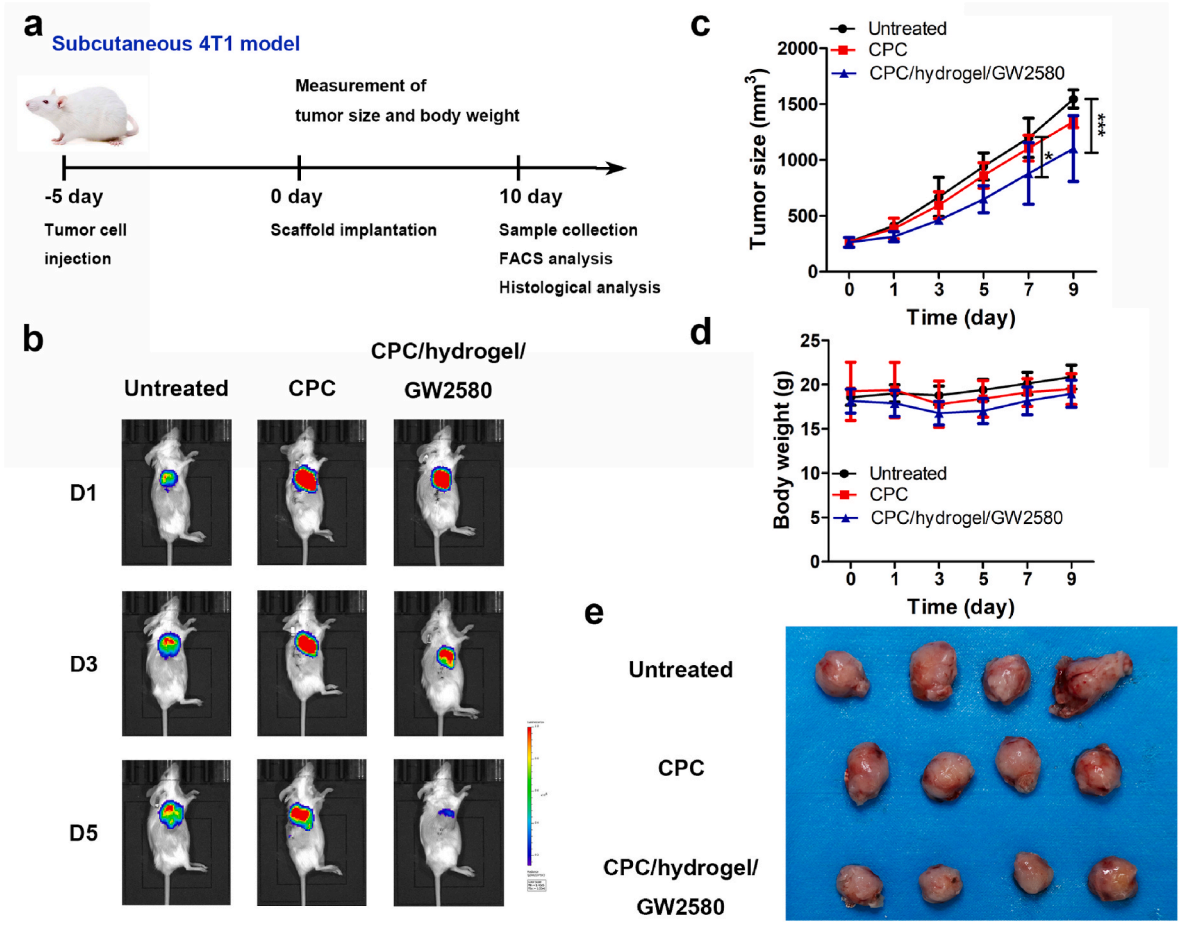

Fig. 6. GW2580-loaded scaffolds effectively inhibit 4T1 breast tumor growth in a mice model. (a) Schematic shows the anti-tumor therapy of inhibitor-loaded scaffolds. (b) IVIS images and (c) tumor size curves show the effect of implanted scaffolds on tumor growth when mice were alive (n = 4, $^{*}P < 0.05$, $^{***}P < 0.001$ vs. Untreated by two-way ANOVA). (d) Body weight measurement results show histocompatibility of the scaffolds (n = 4). (e) Digital photograph of the tumors shows the anti-tumor effect of implanted scaffolds after 10 days of treatment.

activity even at a low concentrations [51]. It has been demonstrated that the inhibition effect may be related to CS interaction with amino groups on osteoclastic mediators (e.g., RANKL) through the sulfonic acid group [52,53]. Additionally, sulfation of glycosaminoglycan was found to significantly inhibit osteoclast differentiation and resorption, and the efficiency depends on the sulfation degree [54]. Furthermore, our previous study revealed that the oxidation process did not change the molecular structure of sulfonic acid group and interfere with the biological function [55].

3.4. Regulation of macrophage polarization

A previous study reported that M0 macrophages could be polarized into M2 type after inducing-culture by IL-10 and IL-4 [56]. Therefore, the scaffold extract medium containing MCSF, IL-10, and IL-4 was prepared to analyze the inhibitory effect of GW2580 loaded scaffolds on M2-polarization of macrophage (Fig. 4a). The cells were collected for phenotypic assays after incubating in the extract medium for 24 h. According to the FACS assay results (Fig. 4b and c), macrophages in the control group were effectively polarized into the M2 type after inducing culture with MCSF, IL-10 and IL-4. The $CD206^{+}$ M2 macrophages proportion was much lower in the CPC/hydrogel/GW2580 group than in other groups ($P < 0.01$).

The RT-PCR assay results were consistent with the FACS results (Fig. 4d). Cells in the CPC/hydrogel/GW2580 group showed lower genes expression of M2 macrophages (CD206 and CD163) and higher genes expression of M1 macrophages (IL-1β and iNOS) when compared to the control group ($P < 0.001$); thus, indicating the polarize-inhibiting effect. Furthermore, the inhibitory effect was found to be highly related to the GW2580 loading dose. Cells cultured in the high dose group showed lower gene expression of M2 macrophages and higher gene expression of M1 macrophages than in the low dose group. These results demonstrated that CSF-1R inhibitor-loaded scaffolds could inhibit the polarization of primary macrophages to M2 type in a GW2580 concentration-dependent approach. Though less effective than the CPC/hydrogel/GW2580 group, the CPC/hydrogel group partially inhibited the M2-polarization of macrophages. In section 3.3, the CPC/hydrogel group was hypothesized to block CSF-1R pathway by competitive binding to inducing cytokines. Polarization inhibition effect of CPC/hydrogel scaffolds may be associated to the competitive binding of released OCS with MCSF, IL-10 and IL-4, which interfered with the binding to macrophages for phenotype modulation.

3.5. Effect on mBMSCs function

Apart from the anti-tumor property, a scaffold for bone tumor postoperative treatment was supposed to promote bone regeneration [13]. Herein, the immunoregulatory scaffold was designed to function in a dual-stage process: regulating harmful macrophage immune microenvironment in the early stage and promoting bone regeneration in the later stage. Although CPC based biomaterials were known to promote bone integration with the biomimetic chemical composition and controllable microstructure [32,33], effects of the developed immunoregulatory scaffold on bone regeneration remain unknown. Therefore,

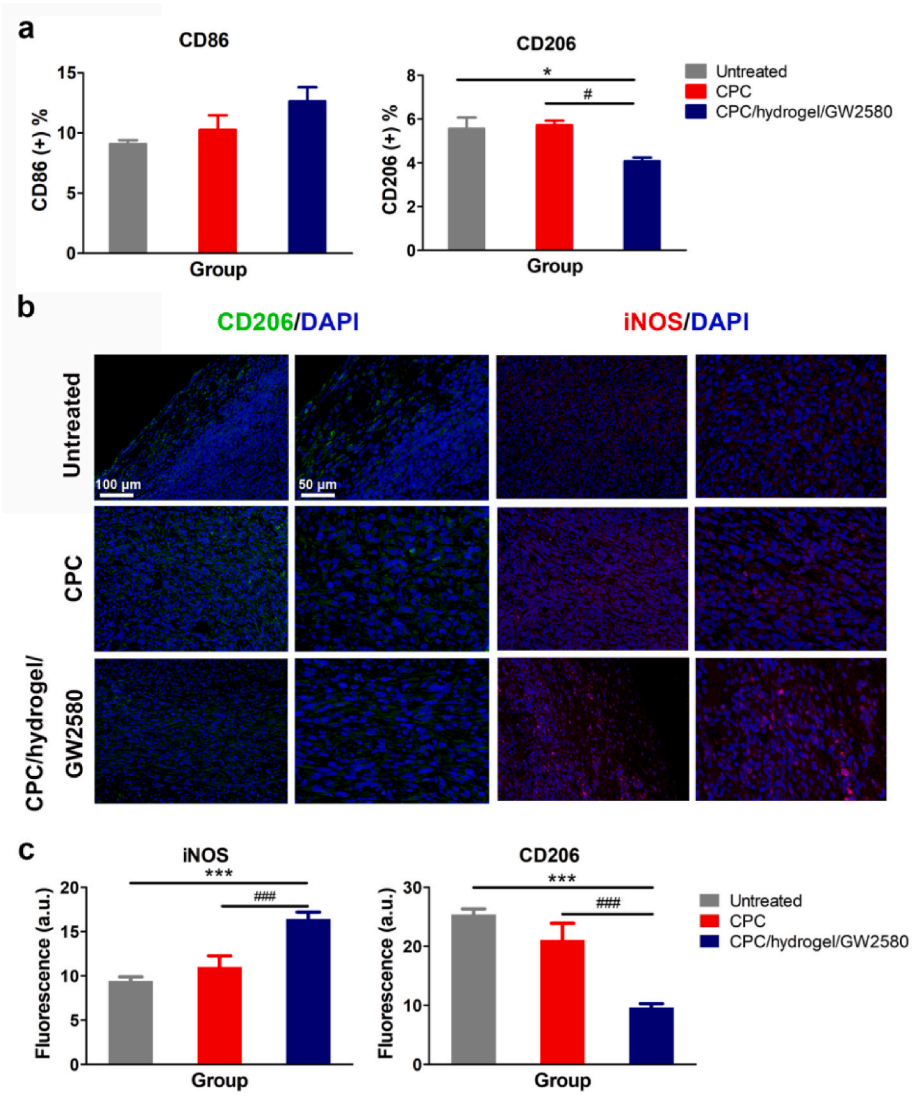

Fig. 7. GW2580-loaded scaffolds effectively regulate polarization of macrophage in 4T1 breast tumor micro-environment *in vivo*. (a) FACS results show M1 ($CD86^+$) and M2 ($CD206^+$) type macrophage ratio in tumors after 10 days of treatment (n = 3, $^*P < 0.05$ vs. Untreated; $\#P < 0.05$ vs. CPC group by one-way ANOVA). (b) Immunofluorescent staining images and (c) related quantitative fluorescence intensity results show distribution of M1 (iNOS) and M2 (CD206) type macrophages in the tumors (n = 3, $^{***}P < 0.001$ vs. Untreated; $\#\#\#P < 0.001$ vs. CPC group by one-way ANOVA).

the influence of scaffolds at the later stage of GW2580 release on proliferation, adhesion, and osteogenic differentiation of mBMSCs was carefully assayed. Fig. 5a shows that mBMSCs had similar proliferation performance after culturing for 24 and 72 h with CPC, CPC/hydrogel, and CPC/hydrogel/GW2580 scaffolds, respectively. No significant differences were observed between the control and scaffold groups. Then, the attachment of mBMSCs to the scaffolds after 72 h of culture was observed under a confocal microscope. Fig. 5b shows that mBMSCs spread better on the HBC/OCS hydrogel coated scaffolds than on CPC scaffolds. However, no substantial differences were observed between the CPC/hydrogel and CPC/hydrogel/GW2580 groups. It was hypothesized that free amino groups of HBC in the hydrogel promoted cell spreading on the scaffolds through charge affinity to the cell membrane. Finally, the effect of scaffolds on the mBMSCs osteogenic differentiation was detected using an ALP kit (Fig. 5c). The results demonstrated that larger ALP-positive areas were induced in the scaffold groups than in the control group. Additionally, no substantial differences were detected among the CPC, CPC/hydrogel, and CPC/hydrogel/GW2580 groups. Therefore, the results suggested that inhibitor-loaded scaffolds did not affect the stem cells function at the later stage of GW2580 release and promoted osteogenesis.

3.6. Immunoregulation and anti-tumor efficacy in vivo

Metastatic and development of bone cancer are closely related to TAMs in the microenvironment [7]. The 4T1 breast tumor, a common *in vivo* model for immunoregulation strategy assessment, was constructed to analyze the therapeutic effect of the immunoregulating scaffolds (Fig. 6a). Tumor-bearing mice were randomly divided into (1) untreated, (2) CPC scaffold, and (3) CPC/hydrogel/GW2580 scaffold groups. The experiments were initiated 5 days after 4T1 cells injection when the tumor reached 100 mm^3. Scaffolds were implanted near the tumor. To detect the anti-tumor effect of the scaffolds, tumor size was assayed with IVIS spectrum and palpation every other day. Fig. 6b shows that the GW2580 loaded scaffolds inhibited tumor growth more efficiently than the untreated and CPC scaffold group. CPC scaffold showed little anti-tumor effect, probably due to physical obstruction. When mice body weights were recorded every 48 h, no substantial differences were observed among the three groups (Fig. 6c), indicating good histocompatibility of the developed scaffolds. Ten days after implantation, the animals were sacrificed, and tumors were excised for general observations, FACS, and histological assays. The images of the collected tumors showed a similar result to the IVIS spectrum images taken before mice were sacrificed. The average tumor size of the CPC/hydrogel/GW2580 group was smaller than that of the other two groups (Fig. 6d).

A FACS assay was further performed to detect effect of GW2580

loaded scaffolds on macrophage phenotype regulation in the tumor. The results revealed that treatment with GW2580 loaded scaffolds significantly reduced the proportion of M2 macrophages ($CD11b^{+}CD206^{+}$) ($P < 0.001$) and increased the proportion of M1 ($CD11b^{+}CD86^{+}$) phenotype macrophages (Fig. 7a). The immunofluorescence histological assay results (Fig. 7b and c) conformed with the FACS results. More $iNOs^{+}$ M1 macrophages and fewer $CD206^{+}$ M2 macrophages were found in the GW2580 loaded scaffold group tumors than in the other two groups ($P < 0.001$). Thus, the GW2580 loaded scaffolds successfully regulated the local M1/M2 macrophage phenotype proportion.

According to previous report [47], the effective dose of GW2580 for tumor growth inhibition is 20–80 mg/kg twice a day orally. With local prolonged release of inhibitor being realized via material design, the GW2580 loaded scaffolds effectively regulated the harmful microenvironment and inhibited tumor growth without affecting normal tissue function at much lower inhibitor loading dose throughout the treatment process.

However, there're expandable points deserve further study. First, GW2580 was here combined with 3D printed scaffolds through electrostatic interaction to prolong its release time. Although GW2580 gradually released in one week and efficiently blocked CSF-1R pathway, stronger bonds can be designed to load the inhibitor on the scaffolds for therapeutic efficiency analysis of inhibitor action time. Second, the loading dose of GW2580 is closely associated with both tumor inhibition and tissue regeneration properties of the scaffolds. Owing to the functional material design, scaffolds containing a relative low dose of GW2580 have been found to effectively regulate macrophage polarization in tumor microenvironment without affecting bone regeneration. In the following study, scaffolds with different loading dose of GW2580 should be prepared to analyze the effect of inhibitor loading dose on postoperative treatment of bone tumor in detail. Third, GW2580 was chosen as a model inhibitor to explore the feasibility of immunoregulatory scaffolds construction for tumor postoperative treatment. Other signal pathway inhibitors or immunoregulatory molecules can be introduced into the scaffolds for drug screening and strategy optimization based on the present data. Fourth, even though we preliminary verified the inhibition effect of immunoregulatory scaffolds on osteoclast formation, the long-term effects in bone tumor postoperative microenvironment and related molecular mechanisms deserve further studies.

4. Conclusions

In this study, 3D printed scaffolds regulating macrophage polarization behavior in the tumor microenvironment were constructed through functional loading of a CSF-1R inhibitor. Bone repair scaffolds were finely printed with a calcium phosphate-based bioink. After concentration optimization, HBC and OCS solutions were evenly coated on the scaffold layer by layer to provide a surface rich in sulfonic acid group for rapid and stable loading of the inhibitor GW2580. *In vitro* results demonstrated that the released inhibitor effectively blocked the CSF-1R pathway, inhibited the M2-type polarization of macrophages, and reprogrammed M2-type to the M1-type. Due to its inhibition of the phosphorylation of CSF-1R and NF-κB pathways, released GW2580 from the scaffolds also significantly inhibited osteoclastogenesis, the important link in the vicious cycle of tumor recurrence and metastasis. At the later stage of GW2580 release, the scaffolds promoted adhesion, spreading, and osteogenic differentiation of mBMSCs, which is promising for bone regeneration. More so, the *in vivo* tumor model verified that GW2580 loaded scaffolds significantly reduced the proportion of M2-type macrophages in tumors and inhibited tumor growth. In conclusion, we proposed a novel postoperative treatment strategy for bone tumors with 3D printed regenerative scaffolds that regulate macrophage immune microenvironment in stages.

CRediT authorship contribution statement

Cuidi Li: Conceptualization, Investigation, Methodology, Data curation, Writing – original draft, Funding acquisition. **Changwei Li:** Investigation, Methodology, Validation, Formal analysis, Data curation. **Zhenjiang Ma:** Investigation, Formal analysis, Methodology. **Hongfang Chen:** Methodology, Formal analysis. **Huitong Ruan:** Methodology, Formal analysis. **Lianfu Deng:** Resources, Project administration. **Jinwu Wang:** Resources, Supervision, Project administration, Funding acquisition. **Wenguo Cui:** Conceptualization, Visualization, Supervision, Project administration, Writing – review & editing, Funding acquisition.

Declaration of competing interest

The authors declare that they have no known competing financial interests or personal relationships that could have appeared to influence the work reported in this paper.

Acknowledgements

This investigation was supported by the National Key Research and Development Program of China (2019YFA0112000 and 2018YFB1105600), National Natural Science Foundation of China (82102210), the Foundation of National Facility for Translational Medicine (Shanghai) (TMSK-2020-117) and GuangCi Professorship Program of Ruijin Hospital Shanghai Jiao Tong University School of Medicine. The authors would like to thank Dr Leilei Chang for her support during the *in vitro* experiments.

Appendix A. Supplementary data

Supplementary data to this article can be found online at https://doi.org/10.1016/j.bioactmat.2022.04.028.

References

[1] L. Xu, H. Qin, Z. Cheng, W.B. Jiang, J. Tan, X. Luo, W. Huang, 3D-printed personalised prostheses for bone defect repair and reconstruction following resection of metacarpal giant cell tumours, Ann. Transl. Med. 9 (2021) 1421.
[2] S.V. Murphy, P. De Coppi, A. Atala, Opportunities and challenges of translational 3D bioprinting, Nat. Biomed. Eng. 4 (2020) 370–380.
[3] J. Zhou, Z. Zhang, J. Joseph, X. Zhang, B.E. Ferdows, D.N. Patel, W. Chen, G. Banfi, R. Molinaro, D. Cosco, N. Kong, N. Joshi, O.C. Farokhzad, C. Corbo, W. Tao, Biomaterials and nanomedicine for bone regeneration: progress and future prospects, Explorations 1 (2021), 20210011.
[4] S. Vanaei, M.S. Parizi, S. Vanaei, F. Salemizadehparizi, H.R. Vanaei, An overview on materials and techniques in 3D bioprinting toward biomedical application, Eng. Regen. 2 (2021) 1–18.
[5] X.J. Shao, S.F. Xiang, Y.Q. Chen, N. Zhang, J. Cao, H. Zhu, B. Yang, Q. Zhou, M. D. Ying, Q.J. He, Inhibition of M2-like macrophages by all-trans retinoic acid prevents cancer initiation and stemness in osteosarcoma cells, Acta Pharmacol. Sin. 40 (2019) 1343–1350.
[6] D.M. Gianferante, L. Mirabello, S.A. Savage, Germline and somatic genetics of osteosarcoma-connecting aetiology, biology and therapy, Nat. Rev. Endocrinol. 13 (2017) 480–491.
[7] A. Mantovani, F. Marchesi, A. Malesci, L. Laghi, P. Allavena, Tumour-associated macrophages as treatment targets in oncology, Nat. Rev. Clin. Oncol. 14 (2017) 399–416.
[8] H. Phuengkham, C. Song, Y.T. Lim, A designer scaffold with immune nanoconverters for reverting immunosuppression and enhancing immune checkpoint blockade therapy, Adv. Mater. 31 (2019), 1903242.
[9] R. Noy, J.W. Pollard, Tumor-associated macrophages: from mechanisms to therapy, Immunity 41 (2014) 49–61.
[10] Y. Zhu, B.L. Knolhoff, M.A. Meyer, T.M. Nywening, B.L. West, J. Luo, A. Wang-Gillam, S.P. Goedegebuure, D.C. Linehan, D.G. DeNardo, CSF1/CSF1R blockade reprograms tumor-infiltrating macrophages and improves response to T-cell checkpoint immunotherapy in pancreatic cancer models, Cancer Res. 74 (2014) 5057–5069.
[11] S.R. Gordon, R.L. Maute, B.W. Dulken, G. Hutter, B.M. George, M.N. McCracken, R. Gupta, J.M. Tsai, R. Sinha, D. Corey, A.M. Ring, A.J. Connolly, I.L. Weissman, PD-1 expression by tumour-associated macrophages inhibits phagocytosis and tumour immunity, Nature 545 (2017) 495–499.
[12] B. Ruffell, N.I. Affara, L.M. Coussens, Differential macrophage programming in the tumor microenvironment, Trends Immunol. 33 (2012) 119–126.

[13] X. Zhang, S. Koo, J.H. Kim, X. Huang, N. Kong, L. Zhang, J. Zhou, J. Xue, M. B. Harris, W. Tao, J.S. Kim, Nanoscale materials-based platforms for the treatment of bone-related diseases, Matter 4 (2021) 2727–2764.
[14] Z. Zhang, J. Zhou, C. Liu, J. Zhang, Y. Shibata, N. Kong, C. Corbo, M.B. Harris, W. Tao, Emerging biomimetic nanotechnology in orthopedic diseases: progress, challenges, and opportunities, Trends Chem 4 (2022) 420–436.
[15] X. Zhang, L. Li, J. Ouyang, L. Zhang, J. Xue, H. Zhang, W. Tao, Electroactive electrospun nanofibers for tissue engineering, Nano Today 39 (2021), 101196.
[16] P.J. Murray, Macrophage polarization, Annu. Rev. Physiol. 79 (2017) 541–566.
[17] A. Sica, A. Mantovani, Macrophage plasticity and polarization: in vivo veritas, J. Clin. Invest. 122 (2012) 787–795.
[18] X. Liu, M. Chen, J. Luo, H. Zhao, X. Zhou, Q. Gu, H. Yang, X. Zhu, W. Cui, Q. Shi, Immunopolarization-regulated 3D printed-electrospun fibrous scaffolds for bone regeneration, Biomaterials 276 (2021), 121037.
[19] A. Kulkarni, V. Chandrasekar, S.K. Natarajan, A. Ramesh, P. Pandey, J. Nirgud, H. Bhatnagar, D. Ashok, A.K. Ajay, S. Sengupta, A designer self-assembled supramolecule amplifies macrophage immune responses against aggressive cancer, Nat. Biomed. Eng. 2 (2018) 589–599.
[20] H. Ruan, Q. Hu, D. Wen, Q. Chen, G. Chen, Y. Lu, J. Wang, H. Cheng, W. Lu, Z. Gu, A dual-bioresponsive drug-delivery depot for combination of epigenetic modulation and immune checkpoint blockade, Adv. Mater. 31 (2019), 1806957.
[21] C. Engblom, C. Pfirschke, M.J. Pittet, The role of myeloid cells in cancer therapies, Nat. Rev. Cancer 16 (2016) 447–462.
[22] B. Ruffell, L.M. Coussens, Macrophages and therapeutic resistance in cancer, Cancer Cell 27 (2015) 462–472.
[23] C.H. Ries, M.A. Cannarile, S. Hoves, J. Benz, K. Wartha, V. Runza, F. Rey-Giraud, Leon P. Pradel, F. Feuerhake, I. Klaman, T. Jones, U. Jucknischke, S. Scheiblich, K. Kaluza, Ingo H. Gorr, A. Walz, K. Abiraj, Philippe A. Cassier, A. Sica, C. Gomez-Roca, Karin E. de Visser, A. Italiano, C. Le Tourneau, J.-P. Delord, H. Levitsky, J.-Y. Blay, D. Rüttinger, Targeting tumor-associated macrophages with anti-CSF-1R antibody reveals a strategy for cancer therapy, Cancer Cell 25 (2014) 846–859.
[24] L. Cai, D. Xu, H. Chen, L. Wang, Y. Zhao, Designing bioactive micro-/nanomotors for engineered regeneration, Eng. Regen. 2 (2021) 109–115.
[25] Z. Wang, W. Kapadia, C. Li, F. Lin, R.F. Pereira, P.L. Granja, B. Sarmento, W. Cui, Tissue-specific engineering: 3D bioprinting in regenerative medicine, J. Contr. Release 329 (2021) 237–256.
[26] J. Yang, X. Zhang, C. Liu, Z. Wang, L. Deng, C. Feng, W. Tao, X. Xu, W. Cui, Biologically modified nanoparticles as theranostic bionanomaterials, Prog. Mater. Sci. 118 (2021), 100768.
[27] C. Liu, H. Shao, F. Chen, H. Zheng, Effects of the granularity of raw materials on the hydration and hardening process of calcium phosphate cement, Biomaterials 24 (2003) 4103–4113.
[28] Q.Q. Wang, M. Kong, Y. An, Y. Liu, J.J. Li, X. Zhou, C. Feng, J. Li, S.Y. Jiang, X. J. Cheng, X.G. Chen, Hydroxybutyl chitosan thermo-sensitive hydrogel: a potential drug delivery system, J. Mater. Sci. 48 (2013) 5614–5623.
[29] B. Zhu, C.Z. Wei, C.L. Hou, Q.S. Gu, D.J. Chen, Preparation and characterization of hydroxybutyl chitosan, E-Polymers 10 (2010) 883–892.
[30] M. Fan, Y. Ma, H. Tan, Y. Jia, S. Zou, S. Guo, M. Zhao, H. Huang, Z. Ling, Y. Chen, X. Hu, Covalent and injectable chitosan-chondroitin sulfate hydrogels embedded with chitosan microspheres for drug delivery and tissue engineering, Mater. Sci. Eng. C 71 (2017) 67–7471.
[31] C. Li, X. Han, Z. Ma, T. Jie, J. Wang, L. Deng, W. Cui, Engineered customizable microvessels for progressive vascularization in large regenerative implants, Adv. Healthc. Mater. (2021), 2101836.
[32] C. Li, Z. Ma, W. Li, T. Jie, L. Zhong, H. Chen, W. Wang, J. Wang, W. Cui, Y. Zhao, 3D-printed Scaffolds Promote Angiogenesis by Recruiting Antigen-specific T Cells. Engineering, 2021.
[33] C. Li, C. Jiang, Y. Deng, T. Li, N. Li, M. Peng, J. Wang, RhBMP-2 loaded 3D-printed mesoporous silica/calcium phosphate cement porous scaffolds with enhanced vascularization and osteogenesis properties, Sci. Rep. 7 (2017), 41331.
[34] T. Koga, M. Inui, K. Inoue, S. Kim, A. Suematsu, E. Kobayashi, T. Iwata, H. Ohnishi, T. Matozaki, T. Kodama, T. Taniguchi, H. Takayanagi, T. Takai, Costimulatory signals mediated by the ITAM motif cooperate with RANKL for bone homeostasis, Nature 428 (2004) 758–763.
[35] M. Peng, Y. Wang, L. Qiang, Y. Xu, C. Li, T. Li, X. Zhou, M. Xiao, J. Wang, Interleukin-35 inhibits TNF-α-induced osteoclastogenesis and promotes apoptosis via shifting the activation from tnf receptor-associated death domain (TRADD)–TRAF2 to TRADD–Fas-associated death domain by JAK1/STAT1, Front. Immunol. 9 (2018).
[36] C. Li, K. Wang, T. Li, X. Zhou, Z. Ma, C. Deng, C. He, B. Wang, J. Wang, Patient-specific scaffolds with a biomimetic gradient environment for articular cartilage-subchondral bone regeneration, ACS Appl. Bio Mater. 3 (2020) 4820–4831.
[37] C. Liu, W. Shen, Y. Gu, Mechanism of hardening process for a hydroxyapatite cement, J. Biomed. Mater. Res. 35 (1997) 75–80.
[38] J. Zhang, H. Zhou, K. Yang, Y. Yuan, C. Liu, RhBMP-2-loaded calcium silicate/calcium phosphate cement scaffold with hierarchically porous structure for enhanced bone tissue regeneration, Biomaterials 34 (2013) 9381–9392.
[39] M.I. El-Gamal, S.K. Al-Ameen, D.M. Al-Koumi, M.G. Hamad, N.A. Jalal, C.-H. Oh, Recent advances of colony-stimulating factor-1 receptor (CSF-1R) kinase and its inhibitors, J. Med. Chem. 61 (2018) 5450–5466.
[40] A. Sica, P. Larghi, A. Mancino, L. Rubino, C. Porta, M.G. Totaro, M. Rimoldi, S. K. Biswas, P. Allavena, A. Mantovani, Macrophage polarization in tumour progression, Semin. Cancer Biol. 18 (2008) 349–355.
[41] A. Sica, T. Schioppa, A. Mantovani, P. Allavena, Tumourassociated macrophages are a distinct M2 polarised population promoting tumour progression: potential targets of anti-cancer therapy, Eur. J. Cancer 42 (2006) 717–727.
[42] J.Y. Hung, D. Horn, K. Woodruff, T. Prihoda, C. LeSaux, J. Peters, F. Tio, S. L. Abboud-Werner, Colony-stimulating factor 1 potentiates lung cancer bone metastasis, Lab. Invest. 94 (2014) 371–381.
[43] M.F. Heymann, F. Lézot, D. Heymann, The contribution of immune infiltrates and the local microenvironment in the pathogenesis of osteosarcoma, Cell. Immunol. 343 (2019), 103711.
[44] K. Redlich, J.S. Smolen, Inflammatory bone loss: pathogenesis and therapeutic intervention, Nat. Rev. Drug Discov. 11 (2012) 234–250.
[45] B. Frenkel, A. Hong, S.K. Baniwal, G.A. Coetzee, C. Ohlsson, O. Khalid, Y. Gabet, Regulation of adult bone turnover by sex steroids, J. Cell. Physiol. 224 (2010) 305–310.
[46] M.N. Michalski, L.K. McCauley, Macrophages and skeletal health, Pharmacol. Therapeut. 174 (2017) 43–54.
[47] J.G. Conway, B. McDonald, J. Parham, B. Keith, D.W. Rusnak, E. Shaw, M. Jansen, P. Lin, A. Payne, R.M. Crosby, J.H. Johnson, L. Frick, M.-H.J. Lin, S. Depee, S. Tadepalli, B. Votta, I. James, K. Fuller, T.J. Chambers, F.C. Kull, S. D. Chamberlain, J.T. Hutchins, Inhibition of colony-stimulating-factor-1 signaling in vivo with the orally bioavailable cFMS kinase inhibitor GW2580, Proc. Natl. Acad. Sci. U.S.A. 102 (2005), 16078.
[48] G.R. Mundy, Metastasis to bone: causes, consequences and therapeutic opportunities, Nat. Rev. Cancer 2 (2002) 584–593.
[49] A. Maurizi, N. Rucci, The osteoclast in bone metastasis: player and target, Cancers 10 (2018) 218.
[50] D. Goltzman, Osteolysis and cancer, J. Clin. Invest. 107 (2001) 1219–1220.
[51] T. Miyazaki, S. Miyauchi, A. Tawada, T. Anada, S. Matsuzaka, O. Suzuki, Chondroitin sulfate-e enhances osteoblast differentiation and inhibits osteoclast differentiation in vitro, Bone 44 (2009) S314.
[52] W. Ariyoshi, T. Takahashi, T. Kanno, H. Ichimiya, K. Shinmyouzu, H. Takano, T. Koseki, T. Nishihara, Heparin inhibits osteoclastic differentiation and function, J. Cell. Biochem. 103 (2008) 1707–1717.
[53] K. Shinmyouzu, T. Takahashi, W. Ariyoshi, H. Ichimiya, S. Kanzaki, T. Nishihara, Dermatan sulfate inhibits osteoclast formation by binding to receptor activator of NF-κB ligand, Biochem. Biophys. Res. Commun. 354 (2007) 447–452.
[54] J. Salbach, S. Kliemt, M. Rauner, T.D. Rachner, C. Goettsch, S. Kalkhof, M. von Bergen, S. Möller, M. Schnabelrauch, V. Hintze, D. Scharnweber, L.C. Hofbauer, The effect of the degree of sulfation of glycosaminoglycans on osteoclast function and signaling pathways, Biomaterials 33 (2012) 8418–8429.
[55] C. Li, K. Wang, X. Zhou, T. Li, Y. Xu, L. Qiang, M. Peng, Y. Xu, L. Xie, C. He, B. Wang, J. Wang, Controllable fabrication of hydroxybutyl chitosan/oxidized chondroitin sulfate hydrogels by 3D bioprinting technique for cartilage tissue engineering, Biomed. Mater. 14 (2019), 025006.
[56] S. Gao, C. Li, Y. Zhu, Y. Wang, A. Sui, Y. Zhong, B. Xie, X. Shen, PEDF mediates pathological neovascularization by regulating macrophage recruitment and polarization in the mouse model of oxygen-induced retinopathy, Sci. Rep. 7 (2017) 42846.